PAPER

^{17}O solid state NMR as a valuable tool for deciphering reaction mechanisms in mechanochemistry: the case study on the ^{17}O-enrichment of hydrated Ca-pyrophosphate biominerals†

Ieva Goldberga, [ID] *[a] Nicholai D. Jensen,[a] Christèle Combes, [ID] [b] Frédéric Mentink-Vigier, [ID] [c] Xiaoling Wang, [ID] [c] Ivan Hung, [ID] [c] Zhehong Gan, [ID] [c] Julien Trébosc, [ID] [d] Thomas-Xavier Métro, [ID] [e] Christian Bonhomme, [ID] [f] Christel Gervais [ID] [f] and Danielle Laurencin [ID] *[a]

The possibility of enriching in ^{17}O the water molecules within hydrated biominerals belonging to the Ca-pyrophosphate family was investigated, using liquid assisted grinding (LAG) in the presence of ^{17}O-labelled water. Two phases with different hydration levels, namely triclinic calcium pyrophosphate dihydrate ($Ca_2P_2O_7 \cdot 2H_2O$, denoted *t*-CPPD) and monoclinic calcium pyrophosphate tetrahydrate ($Ca_2P_2O_7 \cdot 4H_2O$, denoted *m*-CPPT β) were enriched in ^{17}O using a "post-enrichment" strategy, in which the non-labelled precursors were ground under gentle milling conditions in the presence of stoichiometric quantities of ^{17}O-enriched water (introduced here in very small volumes ∼10 μL). Using high-resolution ^{17}O solid-state NMR (ssNMR) analyses at multiple magnetic fields, and dynamic nuclear polarisation (DNP)-enhanced ^{17}O NMR, it was possible to show that the labelled water molecules are mainly located at the core of the crystal structures, but that they can enter the lattice in different ways, namely by dissolution/recrystallisation or by diffusion. Overall, this work sheds light on the

[a]ICGM, Université de Montpellier, CNRS, ENSCM, Montpellier, France. E-mail: ieva.goldberga@umontpellier.fr; danielle.laurencin@umontpellier.fr

[b]CIRIMAT, Université de Toulouse, CNRS, Toulouse INP – ENSIACET, Toulouse, France
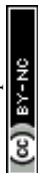
[c]National High Magnetic Field Laboratory (NHMFL), Tallahassee, Florida, USA

[d]Université de Lille, CNRS, INRAE, Centrale Lille, Université d'Artois FR2638 – IMEC – Institut Michel Eugène Chevreul, 59000 Lille, France

[e]IBMM, Université de Montpellier, CNRS, ENSCM, Montpellier, France

[f]LCMCP, UMR 7574, Sorbonne Université, CNRS, Paris, France

importance of high-resolution ^{17}O NMR to help decipher the different roles that water can play as a liquid-assisted grinding agent and as a reagent for [17]O-isotopic enrichment.

Introduction

Despite the increasing number of mechanochemical synthetic procedures being developed to prepare molecular and materials systems, the exact details of how reactions occur are still unclear in many cases. Most frequently, ball-milling (BM) reactions are performed in closed jars, where the course of the reaction is followed by stopping the milling process, and analysing the reaction medium using techniques like powder X-ray diffraction (pXRD) and IR/Raman spectroscopies. Yet, such analyses are often insufficient when studying the formation and nature of amorphous or disordered intermediates, as they cannot provide straightforward identification of these species. *A contrario*, because it is sensitive to the local environment of nuclei, solid-state NMR (ssNMR) is a highly valuable approach for helping determine the nature of amorphous/disordered compounds. As such, it is no surprise that there are an increasing number of examples in which ssNMR has been used to help understand reaction mechanisms in ball-milling.[1] Among representative works, one can cite (i) the study by Baxter *et al.* on the mechanochemical amorphisation of cadmium based ZIFs using ^{13}C, ^{15}N and [113]Cd ssNMR;[2] and (ii) the studies by MacKenzie and co-workers on the mechanochemical synthesis and also amorphisation of aluminosilicates like mullite, using ^{27}Al ssNMR.[3]

Oxygen-17 stands out as a highly attractive probe for gaining deep insight into the composition of reaction media in ball-milling *via* ssNMR. Indeed, its chemical shift scale exceeds 1000 ppm (against only ∼200 ppm in the case of ^{13}C). Furthermore, oxygen-17 ssNMR also offers the possibility of reaching complementary information on the local bonding environment of oxygen by measuring the [17]O-quadrupolar parameters, as the spin of [17]O is 5/2.[4] The first evidence of the interest in using high-resolution ^{17}O ssNMR (as well as MAS-DNP – magic angle spinning dynamic nuclear polarisation) to investigate reaction mechanisms in ball-milling was provided by Chen *et al.*, who looked into the formation of chemical bonds between reacting silica and titania particles and provided evidence of the formation of Ti–O–Si bridges after only 3 minutes of milling.[5] Subsequently, Leroy *et al.* demonstrated that ^{17}O ssNMR analyses could provide valuable insight into the structure of Zn-terephthalate phases, isolated in pure form using ball-milling and *operando* analyses of the reaction medium.[6] Lastly, in a recent investigation by Goldberga *et al.*, it was shown that the water molecules within calcium oxalate hydrates could be enriched in [17]O, further enabling to investigate the dynamics of the water molecules within these crystalline phases.[7] Moreover, the isotopic labelling of the water molecules in ^{2}H and [18]O was also performed as part of the same work. This particular isotopic enrichment was used to help rationalise the reaction mechanisms occurring in ball-milling during the isotopic labelling, by showing that the enrichment process predominantly occurred by a dissolution–recrystallisation mechanism.

Beyond enabling a better understanding of ball-milling reactions, the possibility of using mechanochemistry to enrich water molecules in [17]O within hydrated materials, like calcium oxalate monohydrate, is very attractive. Many of

the minerals found in natural environments contain "water"; however, the exact way in which these molecules can enter, stabilise or affect the properties of different crystal structures is often unclear and requires investigation.[8] This is particularly the case for the water molecules within the biomineral phases present in living organisms. For instance, different phases of hydrated calcium pyro-phosphates with a general formula of $Ca_2P_2O_7 \cdot nH_2O$ (with $n = 0, 1, 2, 3$, and 4) have been reported and studied, some of which are known to be part of patho-logical calcifications which can form in joints (in diseases like pseudo-gout).[9] Even for the most studied dihydrate and tetrahydrate forms, their crystallisation and interconversion still need to be clarified. Thus, high-resolution ^{17}O NMR appears as a desirable tool for looking more specifically at the water molecules in the crystal structures. However, the very high cost of ^{17}O-enriched water (up to more than 2000 € per mL for water enriched at 90% in ^{17}O) makes preparing such compounds prohibitively expensive when using standard precipitation condi-tions in an aqueous solution. This explains why this analytical technique has never been used so far for studying such phases. Being able to carry out the ^{17}O-isotopic labelling by engaging only microlitre quantities of enriched water, as recently done for calcium oxalate monohydrate (COM) and calcium oxalate dihydrate (COD),[7] thus appears highly attractive.

This manuscript aims to investigate how ball-milling can be used to enrich water molecules found in hydrated Ca-pyrophosphates in oxygen-17. The focus was mainly set on the labelling of two crystalline phases (Fig. 1): monoclinic $Ca_2P_2O_7 \cdot 4H_2O$ (*m*-CPPT, under its β form) and triclinic $Ca_2P_2O_7 \cdot 2H_2O$ (*t*-CPPD). First, the ball-milling conditions were optimised in view of the enrichment, using various analytical techniques, including pXRD and ^{31}P ssNMR. Then, the isotopic enrichment in ^{17}O was investigated using ssNMR as well as MAS-DNP analyses, and experimental ^{17}O MAS NMR spectra were compared to those calculated from GIPAW-DFT methods. From a more general perspective, how such experiments and characterisations can help inform on reaction mechanisms in ball-milling is discussed.
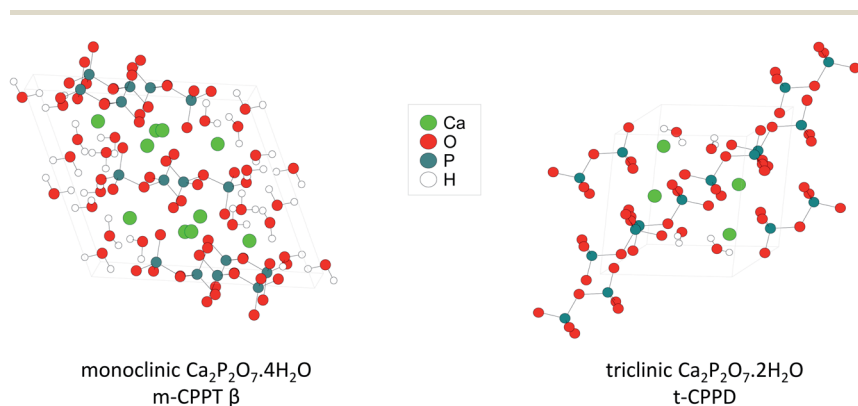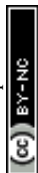

monoclinic $Ca_2P_2O_7.4H_2O$
m-CPPT β

triclinic $Ca_2P_2O_7.2H_2O$
t-CPPD

Fig. 1 Representation of the crystal structures of the two calcium pyrophosphate hydrates enriched in ^{17}O as part of this work.

Experimental section

Reagents and synthetic equipment

Monoclinic calcium pyrophosphate tetrahydrate (m-CPPT β, $Ca_2P_2O_7 \cdot 4H_2O$), and triclinic calcium pyrophosphate dihydrate (t-CPPD, $Ca_2P_2O_7 \cdot 2H_2O$) were synthesised by following or adapting previously published procedures.[9] $H_2^{17}O$ (∼40% or ∼90% ^{17}O enrichment) was purchased from CortecNet and used as received. All milling experiments were carried out in a Retsch Mixer Mill MM400 apparatus operated at room temperature (22 ± 4 °C). Polytetrafluoroethylene (PTFE) balls (10 mm diameter) with a stainless-steel core were purchased from Retsch. Milling jars, beads, and micro-syringes (used to introduce the labelled water) were dried under vacuum before use.

Labelling of calcium pyrophosphate tetrahydrate (m-CPPT β)

One PTFE ball with a stainless-steel core was placed in a 10 mL stainless steel grinding jar (with a screw-top lid). Non-labelled m-CPPT β (60 mg, ∼0.2 mmol) was then added. Isotopically enriched water (14 μL, ∼0.8 mmol) was then deposited on the reactor's wall. The jar was closed, sealed with parafilm and subjected to grinding for 5 minutes in the mixer mill operated at 25 Hz. The material was then recovered by gentle scraping of the jar walls and dried under vacuum for 5 minutes to remove excess water. The sample (m = 58 mg) was stored in a parafilmed glass vial placed in a container with molecular sieves at −16 °C until further use. Prior to any characterisation by pXRD, SEM, and ^{17}O NMR spectroscopy, samples were taken out of the freezer and left thawing for 30 minutes.

Labelling of calcium pyrophosphate dihydrate (t-CPPD)

One PTFE ball with a stainless-steel core was placed in a 10 mL stainless steel grinding jar (with a screw-top lid), followed by t-CPPD (60 mg, ∼0.2 mmol), and finally, ^{17}O-enriched water (7 μL, ∼0.4 mmol) was deposited on the reactor's wall. The jar was closed, sealed with parafilm and subjected to grinding for 5 minutes in the mixer mill operated at 25 Hz. The material was then recovered by gentle scraping of the jar walls and dried under vacuum (m = 55 mg). The sample was stored under the same conditions as labelled m-CPPT β.

Powder X-ray diffraction (pXRD) and scanning electron microscopy (SEM) characterisations

pXRD analyses were performed on an X'Pert MPD diffractometer using CuK$_{\alpha 1}$ radiation (λ = 1.5406 Å) with the operating voltage and current maintained at 40 kV and 25 mA, respectively. X-ray diffractograms were recorded between 5° and 60° in 2θ, with a step size of 0.017° (with count time per step of ∼50 s).

SEM analyses were carried out on a Zeiss Evo HD15 scanning electron microscope equipped with an Oxford Instruments X-MaxN SDD 50 mm² EDXS detector. Before the SEM analyses, samples were deposited on double-sided conducting carbon tape and then metallised with carbon.

^{31}P solid-state NMR experiments

The ^{31}P NMR experiments were performed at 7.0 and 14.1 T on Varian VNMRS spectrometers (ICGM, France), using 3.2 mm HX or HXY probes, operating at
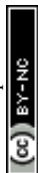
[31]P Larmor frequencies of 121.44 and 242.82 MHz, respectively. Samples were spun at a frequency of 8 kHz (without temperature regulation). [1]H–[31]P cross-polarisation (CP) MAS (Magic Angle Spinning) NMR experiments were performed at 7.0 T using [1]H 90° pulse of 2.5 μs, and a contact time of 3 ms, using a ramped pulse on ^{1}H, and a square pulse on [31]P. During acquisition, SPINAL-64 ^{1}H decoupling was used.[10] Further experimental details are given in Table S1.† A CP-INADEQUATE (Incredible Natural Abundance Double Quantum Transfer Experiment)[11] ^{31}P MAS NMR experiment was also carried out at 14.1 T on the *t*-CPPD phase after milling. [31]P chemical shifts were referenced to hydroxyapatite at 2.8 ppm.

^{17}O solid-state NMR experiments

Oxygen-17 solid-state NMR (ssNMR) spectra were recorded at multiple magnetic fields (B_0 = 9.4, 14.1, 18.8 and 35.2 T) at different NMR facilities (ICGM in Montpellier, UCCS in Lille and MagLab in Tallahassee). [17]O chemical shifts were referenced using tap water at 0.0 ppm (or D_2O at −2.7 ppm).

^{17}O ssNMR experiments were performed at 9.4 and 14.1 T on Varian VNMRS spectrometers (ICGM, France), using 3.2 mm HX or HXY probes, operating at [17]O Larmor frequencies of 54.18 and 81.31 MHz, respectively. Samples were spun at the magic angle, at a frequency of 18 kHz, and with temperature regulated at 0 °C. The 1D ^{17}O MAS (Bloch decay) NMR experiments were performed using a 1.0 μs excitation pulse (which would be a 30° tilt angle on a liquid). The double-frequency sweep (DFS)[12] enhancement scheme was used in some of the experiments. The experimental parameters were as follows: DFS pulse of 500 μs (with RF of ∼10 kHz), with a sweep width between 80 and 200 kHz, followed by an excitation pulse of 1.0 μs. SPINAL-64 ^{1}H decoupling was applied in some experiments. Other details, such as the RF power used for decoupling, recycle delays, and the number of transients, are reported in Table S1.† An additional DFS-echo ^{17}O MAS NMR experiment was recorded for the *m*-CPPT β phase at 100 K using the 14.1 T MAS-DNP instrument of the MagLab in Tallahassee (operated without microwave irradiation),[13] and spinning at 13 kHz. The echo delay was set to 1 rotor period, the recycle delay used was 1 s, and the number of scans acquired was 4096.

At 18.8 T, ^{17}O MAS NMR spectra were recorded on a Bruker Avance NEO NMR spectrometer (UCCS, France) equipped with a 3.2 mm HX probe operating at [17]O and ^{1}H frequencies of 108.46 MHz and 800.12 MHz, respectively. The spinning frequency was controlled at 16 kHz, with the temperature regulated at 0 °C. The 1D ^{17}O MAS (Bloch decay) NMR experiment was performed using a 1.0 μs pulse for excitation (corresponding to a 22.5° tilt angle on a liquid). The recycle delays and number of transients acquired in each experiment can be found in Table S1.†

At 35.2 T, ^{17}O MAS NMR analyses were performed using the SCH magnet[14] at the NHMFL (Maglab, USA) on a Bruker Avance NEO NMR spectrometer equipped with a 3.2 mm single-resonance MAS probe operating at a [17]O frequency of 203.36 MHz. The spinning frequency was set to 18 kHz with temperature control at +10 °C. The 1D [17]O Hahn echo experiment was recorded using one rotor period with a π/2 and π pulse lengths of 5.0 and 10.0 μs, respectively. No ^{1}H decoupling was applied for this experiment. The recycle delay and number of transients acquired can be found in Table S1.†

^{17}O dynamic nuclear polarisation NMR

The MAS-DNP experiments were carried out in Tallahassee on a 14.1 T magnet equipped with the gyrotron operating at 395.17 GHz with 12 W power.[13] The temperature for VT/bearing/drive gas was 92/100/105 K and 98 K without microwave irradiation, and the sample was spun at 13 kHz. The labelled m-CPPT β sample was impregnated with a 10 mM solution of AMUPol[15] in d^8-glycerol/D$_2$O/H$_2$O (6/3/1 %v) (about 15 mg of m-CPPT β impregnated with 9 μL of AMUPol solution), and packed into a 3.2 mm sapphire rotor. It should be noted that impregnation with another radical solution (13 mM TEKPol in 1,1,2,2-tetrachloroethane) did not generate hyperpolarisation on m-CPPT β. Three freeze–thaw cycles were applied to the sample before insertion into the probe. The packed rotor was also prespun using a benchtop spinner at room temperature to ensure stable spinning. The enhancement was $\varepsilon_{on/off} \approx 25$ and the build-up $T_B \approx$ 4 s. For m-CPPT β, the ^{17}O{^{1}H} DNP CPMAS experiments were then performed on a 3.2 mm HXY probe using HCO configuration. The initial ^{1}H CP 90° pulse was 2.5 μs, and a contact time of 1.5 ms with ∼100 kHz RF field was used. SPINAL-64 ^{1}H decoupling was applied during acquisition (∼100 kHz). The recycle delay was set to 5 s, and the number of scans acquired was 10 150.

To ensure the signals measured arise from m-CPPT β only, we measured the natural abundance of ^{17}O arising from the DNP matrix alone. 30 μL of the solution was packed into a sapphire rotor which led to an enhancement of 150. Under these conditions, natural abundance ^{17}O signals could be detected, but their intensity was a fraction of the signals measured for the impregnated m-CPPT β.

Lastly, it is worth mentioning that the DFS-echo ^{17}O NMR spectrum of the impregnated m-CPPT β phase was also recorded at 100 K (in the absence of DNP), using a recycle delay of 0.5 s, and acquiring 4096 scans. No significant difference was observed compared to the non-impregnated material.

Computational studies, including ^{17}O GIPAW-DFT calculations of NMR parameters

Geometry optimisations for m-CPPT β and t-CPPD structures were carried out using the crystallographic data reported in the literature, as in our previous experimental/computational study on calcium pyrophosphates, which corresponds to 92 atoms per m-CPPT β structure relaxation, and 34 for t-CPPD.[9] First, the missing protons were added to the structures. Atomic positions were then relaxed using the Vienna ab initio simulation package (VASP),[16] based on the Kohn–Sham density functional theory (DFT), and using a plane-wave pseudopotential approach with an energy cut-off of 600 eV and 2 × 2 × 2 or 3 × 3 × 3 k-point mesh for m-CPPT β and t-CPPD, respectively. During the geometry optimisation, unit cell parameters were kept fixed to ensure consistency between the experimental and optimised structures. Structural optimisations were performed by relaxing H positions only, as in our previous study on calcium pyrophosphates.[9c]

NMR parameters were calculated for all structures using the QUANTUM-ESPRESSO code,[17] keeping the atomic positions equal to the values previously determined using VASP. The Perdew–Burke–Ernzerhof (PBE) generalised gradient approximation was used,[18] and the valence electrons were described by norm-conserving pseudopotentials[19] in the Kleinman–Bylander form.[20] The shielding tensor was computed using the GIPAW approach.[21] The wave functions were
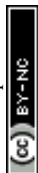
expanded on a plane wave basis set with a kinetic energy cut-off of 80 Ry. The calculations were done using the same k-space mesh density as for relaxation.

The isotropic chemical shift δ_{iso} is defined as $\delta_{iso} \approx -(\sigma - \sigma_{ref})$, where σ is the isotropic shielding and σ_{ref} is the isotropic shielding for the same nucleus using a hydrate reference system, in a similar way as in our previous work on calcium oxalate monohydrate.[7] For these hydrates, the maximum deviation between experimental and DFT-calculated ^{17}O isotropic shifts was found to be 6 ppm.[7] The quadrupolar moments (Q) used to calculate the C_Q of ^{17}O was -2.558 fm^2.[22] Calculated values are reported in Table S2 (ESI†).

Results and discussion

Similar liquid-assisted grinding (LAG) conditions as reported previously for the labelling of COM[7] were used: 60 mg of calcium pyrophosphate hydrate were milled for just 5 minutes at 25 Hz in the presence of microlitre-quantities of water ($\sim$7 and 14 μL for t-CPPD and m-CPPT β, respectively), using a stainless-steel reactor containing 1 PTFE-coated bead. After the reaction, the products were characterised by various techniques, including pXRD and scanning electron microscopy (SEM). These milling conditions were initially tested using non-labelled water, before switching to ^{17}O-enriched water.

As shown in Fig. 2, in the case of m-CPPT β, particles with platelet-morphology were still observed after 5 minutes of milling, and the pXRD pattern essentially resembled that of the starting material, with only some changes in relative intensity of diffraction peaks due to modifications in the particle morphology and packing (thereby affecting the preferential orientation effects apparent in pXRD analyses). Regarding t-CPPD, although pXRD analyses also showed that the compound remained crystalline after the milling, more careful analyses of the baseline of the patterns suggested that small traces of
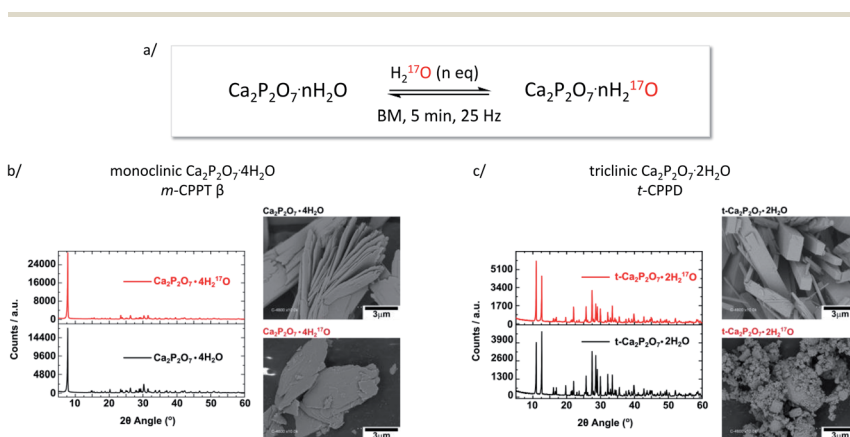

Fig. 2 (a) Scheme showing the equilibration conditions used for the isotopic enrichment of water molecules in m-CPPT β and t-CPPD phases using ball-milling (only a fraction of the ^{17}O-enriched water replaces non-labelled water molecules initially present in the lattice); (b) pXRD and SEM analyses of m-CPPT β before and after BM; (c) pXRD and SEM analyses of t-CPPD before and after BM. An expansion of the pXRD patterns of t-CPPD before and after milling is shown in Fig. S1 (ESI†).
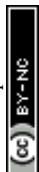
the monoclinic calcium pyrophosphate dihydrate polymorph ($Ca_2P_2O_7 \cdot 2H_2O$, denoted *m*-CPPD) may be present, as shown in Fig. S1 (ESI†). Moreover, SEM images revealed a much more pronounced change in particle morphology compared to *m*-CPPT β.

As pXRD informs on the crystalline phases present in materials, complementary ^{31}P NMR analyses were carried out under magic angle spinning (MAS). As can be seen in Fig. 3, in the case of *m*-CPPT β, the spectrum after milling was essentially the same as the one of the starting material. This shows that neither crystalline impurities nor amorphous by-products were formed during the milling. Concerning *t*-CPPD, in addition to the signals expected for pyrophosphates in a crystalline *t*-CPPD phase,[9c] an additional resonance at ∼−9.9 ppm could be observed. A complementary 2D [31]P–[31]P INADEQUATE experiment was performed, showing that this resonance correlates well with another weak-intensity one at ∼−5.9 ppm (see ESI, Fig. S2†). Based on previous ^{31}P MAS NMR analyses of hydrated calcium pyrophosphates,[9c] both resonances belong to the pyrophosphate unit of the *m*-CPPD impurity which was detected in pXRD. It is important to highlight that just like for the *m*-CPPT β phase, no amorphous component could be detected by ^{31}P NMR.

Given that for *m*-CPPT β and *t*-CPPD the milling conditions were gentle enough to maintain the crystallinity of the starting materials, with only very limited transformation into other hydrates, ^{17}O NMR analyses were performed. The ^{17}O MAS NMR spectra of the isolated phases are shown in Fig. 4. Due to the quadrupolar nature of oxygen-17, these analyses were performed at different magnetic fields (9.4, 14.1, 18.8 T and 35.2 T). For both compounds, a broad asymmetric ^{17}O NMR signal was observed in just a few hours, which is consistent with what one may expect for water molecules within solid environments.[7] This is especially evident when measurements at a lower magnetic field are considered, as the second order quadrupolar lineshape becomes more visible (see Fig. 4, analyses at 9.4 and 14.1 T). Importantly, if the added enriched water had stayed under a "liquid" form in the isolated product (for instance, by forming a weakly-bound layer adsorbed at the surface of the crystallites), a much narrower and symmetric signal, centred around 0 ppm, would have been obtained in ^{17}O NMR.
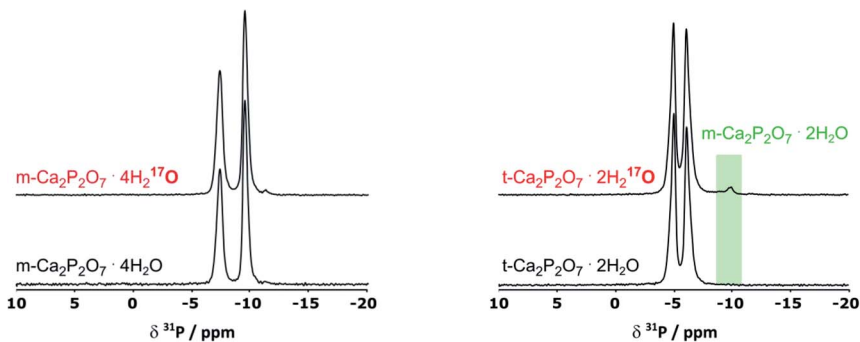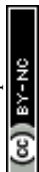

Fig. 3 ^{31}P CPMAS NMR spectra of *m*-CPPT β (left) and *t*-CPPD (right) before and after BM, showing the formation of a new by-product after milling *t*-CPPD, which was identified as *m*-CPPD (green-shaded zone). Only the region with isotropic ^{31}P chemical shifts is shown here.
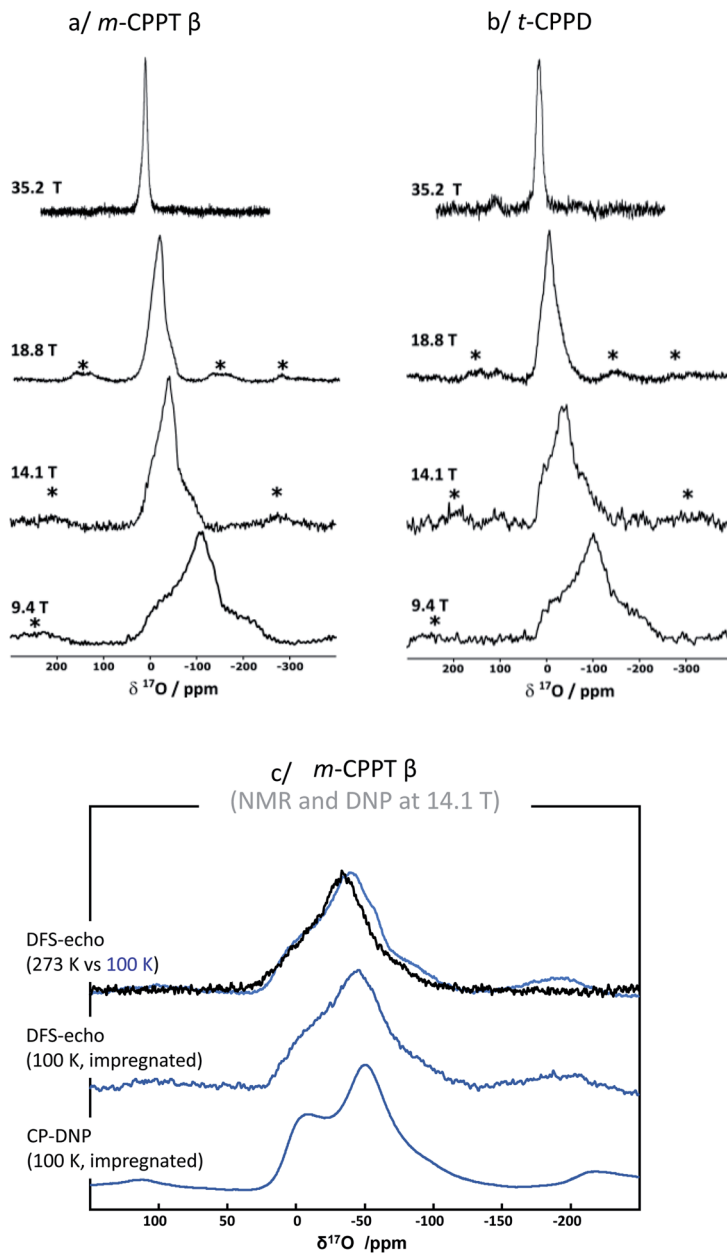
Fig. 4 ^{17}O MAS NMR spectra of (a) m-CPPT β and (b) t-CPPD after ^{17}O-labelling using BM, recorded at different magnetic fields (9.4, 14.1, 18.8 and 35.2 T). Zoom into the lineshapes recorded at 35.2 T is provided in the ESI (Fig. S3†). (c) Low-temperature ^{17}O MAS NMR and DNP-enhanced NMR analyses of the m-CPPT β phase at 14.1 T (see experimental section for details). "*" symbols correspond to spinning sidebands.

Complementary analyses using DNP were also performed on the m-CPPT β phase, showing that its ^{17}O signature mainly comes from the "core-like" enriched water molecules rather than surface ones (see Fig. 4c). Indeed, the DNP spectra
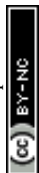
recorded using ^{1}H → ^{17}O CPMAS sequence, in which the ^{1}H are initially excited through the radicals of the impregnating solution (meaning that they are more representative of surface water ^{17}O signature), show a different signature than the direct excitation ^{17}O NMR spectra (recorded with a DFS-echo sequence) obtained at the same field and temperature. Overall, these analyses show that during the liquid-assisted grinding process, the very small amount of labelled water added also plays the role of a *reagent*, enabling the isotopic enrichment to occur, and leading to an overall exchange with non-labelled water molecules initially present in the hydrated crystal structures. Such information could not have been reached in the absence of isotopic labelling of the water molecules.

To further analyse the ^{17}O MAS NMR spectra, *ab initio* calculations of the ^{17}O NMR parameters were performed using the GIPAW-DFT method (see Table S2, ESI†). For each structure, the ^{17}O NMR parameters of the crystallographically inequivalent water molecules in the crystal structure were calculated (calculations being performed at 0 K), and the corresponding ^{17}O MAS NMR spectra were simulated, and compared to the experimental ones. For the *t*-CPPD phase (see ESI Fig. S4†), the overall lineshape calculated for the water molecules reproduces relatively well the experimental one, especially when looking at the breadth of the signal (which mainly arises from the second order quadrupolar broadening). The 2 water sites were not resolved at this stage. Further analyses using Multiple-Quantum Magic Angle Spinning (MQMAS) NMR sequences would be needed for this,[7] which is beyond the scope of the present work. Here, only an *average* isotropic shift δ_{iso} and quadrupolar parameter P_Q were determined for the 2 sites, by considering the change in peak maximum position as a function of the magnetic field (see ESI, Fig. S5†). Nevertheless, the changes in ^{17}O linewidth as a function of the magnetic field reflect the presence of more than one water environment in the material. It is important, however, to highlight that the experimental ^{17}O MAS NMR spectrum of enriched *t*-CPPD is more similar to the one calculated for the *t*-CPPD phase, rather than the *m*-CPPD polymorph (see ESI Fig. S4†), suggesting that the enriched water is mainly located in the core of the former compound (rather than in the less abundant *m*-CPPD by-product which is formed during milling).

Regarding the *m*-CPPT β phase (see ESI, Fig. S6†), the overall experimental lineshape was found to differ more significantly compared to the DFT-calculated one. First, it should be noted that the four crystallographically distinct water sites of *m*-CPPT β could not be resolved using 1D MAS experiments, nor 2D MQMAS experiments (data not shown). At this stage, only an *average* isotropic shift δ_{iso} and quadrupolar parameter P_Q were determined for the water sites, by considering the change in peak maximum position as a function of the magnetic field (see ESI, Fig. S7†). However, it is worth noting that despite the lack of resolution, the evolution of the linewidth as a function of the magnetic field reflects the presence of more than one water site, and preliminary evidence of a higher frequency water resonance can even be noticed at the ultra-high magnetic field (35.2 T data, high-frequency tailing – see orange arrow in Fig. S3a†). The presence of such a signal would be consistent with the GIPAW-DFT calculations, which show a distinct high chemical shift water site (see O_{W1} in Table S2†). Second, it should be highlighted that the experimental ^{17}O NMR spectrum of *m*-CPPT β is clearly narrower than the one calculated by DFT. Such difference can be indicative of rapid reorientations of the water molecules within the crystal structure at room temperature, which
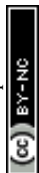
would lead to a partial averaging of the apparent quadrupolar coupling constant in ^{17}O NMR, leading to a difference with the DFT results (as calculations are performed at 0 K). Considering the crystal structure of m-CPPT β (Fig. 1), the observation of such water dynamics at room temperature is actually not fully surprising. Indeed, the water molecules in this structure are all within the same interlayer space (water layer thickness ~4 Å), where they interact with each other through hydrogen-bonding, and are capable of easily changing their local orientation. After ball-milling, the sheet-like morphology of the crystallites is maintained (as shown by SEM, Fig. 2b), and the crystal structure is preserved (as shown by XRD, Fig. 2b), which implies that the enriched water molecules are most likely also present in the hydrated layers and prone to similar motions. As a matter of fact, even after cooling the sample down to 100 K, only a slight broadening of the ^{17}O resonance is observed in NMR, showing that local movements of the water molecules in the interlayer space are still present (see Fig. 4c, top spectra recorded at 273 vs. 100 K).

The ^{17}O NMR analyses also revealed that the ^{17}O-enrichment level was significantly different between the m-CPPT β and t-CPPD phases, despite both samples having been labelled using similar milling conditions. Indeed, ^{17}O MAS NMR spectra of the m-CPPT β phase were systematically obtained with better sensitivity than for the t-CPPD phase, a difference which could not be accounted for by simply considering the difference in the mass percentage of H_2O between both phases (see ESI, Fig. S8,† for a quantitative comparison). The comparison of the crystal structures of the m-CPPT β and t-CPPD phases can explain why such differences in labelling rate are observed by ^{17}O NMR. In the former case, water molecules are all present within a layer, with notably "weak" hydrogen-bonding interactions between them, with one water molecule not coordinated to Ca^{2+}. For t-CPPD, however, no such layered arrangement is observed, and the water molecules appear to be in a more constrained local environment within the crystal structure, with all water molecules coordinated to Ca^{2+} (see ESI, Fig. S9†). Consequently, the ^{17}O labelling of the water molecules in the m-CPPT β structure would be more straightforward, as the enriched water molecules could enter the crystal structure by simple diffusion inside the hydrated layers. In contrast, in the case of the t-CPPD phase, larger structural changes involving partial dissolution/ recrystallisation of the starting material would be needed for the enriched water to enter the crystal structure. This could also explain the partial formation of the m-CPPD by-product, with some of the calcium and pyrophosphate ions adopting a different arrangement upon recrystallisation. To further test this hypothesis, an attempt to enrich both materials by simple "shaking" in the presence of ^{17}O-enriched water (but in the absence of milling beads) was performed, such protocol having been previously tested for COM as well.[7] Only in the case of the m-CPPT β phase was this alternate procedure found to be successful, confirming that the labelling is more straightforward to achieve for this phase, due to its layered structure.

Overall, the different characterisations performed on the ^{17}O-enriched phases, notably using solid state NMR, enable to propose two different mechanisms by which water can react with hydrated biominerals, when performing the liquid-assisted grinding under gentle milling conditions like those described here (5 minutes BM at 25 Hz, using 1 PTFE coated ball). On the one hand, $H_2^{17}O$ can enter the crystal structure by partial dissolution/recrystallisation of the hydrated
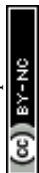
biomineral. This requires rather significant changes at the surface/interface of the crystallites, and can possibly lead to the formation of minority side-products during this process. This is what was observed here for *t*-CPPD, with both significant changes in crystallite morphology after ball-milling (Fig. 2c), and the formation of small amounts of *m*-CPPD polymorph (Fig. 3). On the other hand, $H_2{}^{17}O$ can enter the crystal structure by diffusion, provided that the crystal structure exhibits continuous domains for water incorporation. In such a situation, no complete change in particle morphology is needed for the water to penetrate the crystal structure. The observations made here for *m*-CPPT β suggest that diffusion of labelled water is likely to occur within the hydrated layers easily. Indeed, SEM images show that the sheet-like morphology of the crystallites is essentially preserved after milling. Moreover, ^{17}O-labelling could also be achieved in only 20 s of milling (Fig. S7b†), or even in the absence of milling (shaking experiment), which strongly points to the fact that significant surface reconstruction upon ball-milling is not needed for this material to become labelled in ^{17}O, and that diffusion is a likely mechanism. It is worth noting that in our former work on COM, a dissolution/recrystallisation process had been proposed (notably based on mass-spectrometry analyses),[7] and this is in line with the fact that the calcium oxalate monohydrate structure does not exhibit any water layers nor water channels allowing for diffusion.

Interestingly, for all the biominerals enriched so far (*t*-CPPD, *m*-CPPT β, COM and COD), no formation of a biomineral exhibiting a higher hydration level was observed, despite the addition of stoichiometric amounts of enriched water in the LAG process. For example, in our previous work on COM, the amount of enriched water added could have led to the formation of the dihydrate form COD, but no trace of this phase was observed. Similarly, here, in the case of *t*-CPPD, the amount of enriched water added could have led to the formation of a tetrahydrate form like *m*-CPPT β during the milling, but only minute conversion of *t*-CPPD into the *m*-CPPD was observed experimentally. Attempts to enable further conversion into a tetrahydrate form by increasing the energy input during the milling process were performed in the latter case (15 minutes BM at 25 Hz, using 2 stainless-steel balls), but led to a complete amorphisation of the Ca-pyrophosphate, as demonstrated by pXRD. Although such observations may not be generalisable to other hydrated biominerals, they show that the use of several characterisation tools, including multinuclear NMR, are needed to identify the labelled products and rationalise the labelling mechanism of hydrates.

Conclusion

Using liquid-assisted grinding in presence of ^{17}O-labeled water, two hydrated Ca-pyrophosphate phases, namely *t*-CPPD and *m*-CPPT β, were enriched in ^{17}O. Several characterisations were carried out on the enriched materials, including by ^{17}O NMR analyses at different magnetic fields (up to 35.2 T), and using DNP. Two different enrichment mechanisms were proposed: dissolution/recrystallisation or diffusion of the enriched water inside the crystal lattice. Based on the different analyses performed, and the local environments of the water molecules within the two crystal structures, the former was proposed to be predominant for *t*-CPPD, while the latter for *m*-CPPT β. More generally speaking, similar analyses could help understand in detail how liquid-grinding

Faraday Discussions
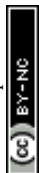
agents like water can interact or react with other crystal structures. From a more practical perspective, the possibility to enrich in ^{17}O biominerals using only microlitre amounts of expensive ^{17}O-enriched water makes LAG a highly attractive approach for future studies on other hydrated biominerals, for which the local environment of water molecules still deserves investigation, as it is the case for canaphite ($CaNa_2P_2O_7 \cdot 4H_2O$),[23] octacalcium phosphate (OCP, $Ca_8($HPO$_4)_2(PO_4)_4 \cdot 5H_2O$),[24] and calcium carbonate hemihydrate ($CaCO_3 \cdot 0.5H_2O$).[25] Further work in the case of canaphite has been initiated, which will be reported in due course. Lastly, it is worth highlighting that beyond the ^{17}O isotopic labelling, similar synthetic procedures would also be worth performing with D_2O (instead of $H_2{}^{17}O$), as ^2H NMR spectroscopy can provide valuable details into the local movements of water molecules within crystal structures and their characteristic frequencies.[7]
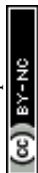
Author contributions

IG, NDJ, TXM and DL carried out the isotopic enrichment experiments, while CC synthesised the hydrated Ca-pyrophosphate precursors. IG and DL carried out the majority of the characterisations by pXRD and solid-state NMR. JT participated in the experiments recorded at 18.8 T in Lille. CB, DL, XW, IH and ZG performed experiments at 35.2 T in Tallahassee. FMV performed the low-temperature ^{17}O NMR and DNP analyses in Tallahassee. IG and CG carried out GIPAW DFT computations. IG and DL wrote the initial draft of the manuscript, and all authors contributed to the final preparation of the article.

Conflicts of interest

There are no conflicts of interest to declare.

Acknowledgements

References

1 C. Leroy, T.-X. Métro and D. Laurencin, The expanding frontier between mechanochemistry & solid state NMR: special focus on inorganic components of materials, in *Comprehensive inorganic chemistry III*, Elsevier, 2023, CH 00136, accepted.

2 E. F. Baxter, T. D. Bennett, A. B. Cairns, N. J. Brownbill, A. L. Goodwin, D. A. Keen, P. A. Chater, F. Blanc and A. K. Cheetham, A Comparison of the Amorphization of Zeolitic Imidazolate Frameworks (ZIFs) and Aluminosilicate Zeolites by Ball-Milling, *Dalton Trans.*, 2016, **45**, 4258–4268.

3 (*a*) M. Schmücker, H. Schneider and K. J. MacKenzie, Mechanical Amorphization of Mullite and Thermal Recrystallization, *J. Non-Cryst. Solids*, 1998, **226**, 99–104; (*b*) S. E. Ashbrook, K. J. D. MacKenzie and S. Wimperis, ^{27}Al Multiple-Quantum MAS NMR of Mechanically Treated Bayerite (α-Al(OH)$_3$) and Silica Mixtures, *Solid State Nucl. Magn. Reson.*, 2001, **20**, 87–99.

4 (*a*) S. E. Ashbrook and M. E. Smith, Solid state ^{17}O NMR—an introduction to the background principles and applications to inorganic materials, *Chem. Soc. Rev.*, 2006, **35**, 718–735; (*b*) G. Wu, ^{17}O NMR studies of organic and biological molecules in aqueous solution and in the solid state, *Prog. Nucl. Magn. Reson. Spectrosc.*, 2019, **114–115**, 135–191.

5 (*a*) C. H. Chen, E. Gaillard, F. Mentink-Vigier, K. Chen, Z. Gan, P. Gaveau, B. Rebière, R. Berthelot, P. Florian, C. Bonhomme, M. E. Smith, T.-X. Métro, B. Alonso and D. Laurencin, Direct isotopic labeling of oxides using mechanochemistry, *Inorg. Chem.*, 2020, **59**, 13050–13066; (*b*) C.-H. Chen, F. Mentink-Vigier, J. Trébosc, I. Goldberga, P. Gaveau, E. Thomassot, D. Iuga, M. E. Smith, K. Chen, Z. Gan, N. Fabregue, T.-X. Métro, B. Alonso and D. Laurencin, Labeling and Probing the Silica Surface Using Mechanochemistry and ^{17}O NMR Spectroscopy, *Chem.–Eur. J.*, 2021, **27**, 12574–12588.

6 C. Leroy, T.-X. Métro, I. Hung, Z. Gan, C. Gervais and D. Laurencin, From operando Raman mechanochemistry to "NMR crystallography": understanding the structures and interconversion of Zn-terephthalate networks using selective ^{17}O-labelling, *Chem. Mater.*, 2022, **34**, 2292–2312.

7 I. Goldberga, N. Patris, C.-H. Chen, E. Thomassot, J. Trébosc, I. Hung, Z. Gan, D. Berthomieu, T.-X. Métro, C. Bonhomme, C. Gervais and D. Laurencin, First Direct Insight into the Local Environment and Dynamics of Water Molecules in the Whewellite Mineral Phase: Mechanochemical Isotopic Enrichment and High-Resolution ^{17}O and ^{2}H NMR Analyses, *J. Phys. Chem. C*, 2022, **126**, 12044–12059.

8 J. M. Griffin, A. J. Berry, D. J. Frost, S. Wimperis and S. E. Ashbrook, Water in the Earth's mantle: a solid-state NMR study of hydrous wadsleyite, *Chem. Sci.*, 2013, **4**, 1523–1538.

9 (*a*) P. Gras, *Etude physico-chimique et structurale de pyrophosphates de calcium hydratés: application aux microcalcifications associées à l'arthrose*, PhD thesis, Université de Toulouse, France, 2014; (*b*) P. Gras, C. Rey, O. Marsan, S. Sarda and C. Combes, Synthesis and Characterisation of Hydrated Calcium Pyrophosphate Phases of Biological Interest, *Eur. J. Inorg. Chem.*, 2013, 5886–5895; (*c*) P. Gras, A. Baker, C. Combes, C. Rey, S. Sarda,
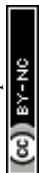
A. J. Wright, M. E. Smith, J. V. Hanna, C. Gervais, D. Laurencin and C. Bonhomme, From crystalline to amorphous calcium pyrophosphates: a solid state nuclear magnetic resonance perspective, *Acta Biomater.*, 2016, **31**, 348–357; (*d*) P. Gras, S. Teychené, C. Rey, C. Charvillat, B. Biscans, S. Sarda and C. Combes, Crystallisation of a highly metastable hydrated calcium pyrophosphate phase, *CrystEngComm*, 2013, **15**, 2294–2300.

10 (*a*) B. M. Fung, A. K. Khitrin and K. Ermolaev, An improved broadband decoupling sequence for liquid crystals and solids, *J. Magn. Reson.*, 2000, **142**, 97–101; (*b*) G. Comellas, J. J. Lopez, A. J. Nieuwkoop, L. R. Lemkau and C. M. Rienstra, Straightforward, Effective Calibration of SPINAL-64 Decoupling Results in the Enhancement of Sensitivity and Resolution of Biomolecular Solid-State NMR, *J. Magn. Reson.*, 2011, **209**, 131–135.

11 (*a*) F. Fayon, D. Massiot, M. H. Levitt, J. J. Titman, D. H. Gregory, L. Duma, L. Emsley and S. P. Brown, Through-space contributions to two-dimensional double-quantum *J* correlation NMR spectra of magic-angle-spinning solids, *J. Chem. Phys.*, 2005, **122**, 194313; (*b*) F. Fayon, G. Le Saout, L. Emsley and D. Massiot, Through-bond phosphorus–phosphorus connectivities in crystalline and disordered phosphates by solid-state NMR., *Chem. Commun.*, 2002, 1702–1703.

12 A. P. M. Kentgens and R. Verhagen, Advantages of Double Frequency Sweeps in Static, MAS and MQMAS NMR of Spin *I*=3/2 Nuclei, *Chem. Phys. Lett.*, 1999, **300**, 435–443.

13 T. Dubroca, A. N. Smith, K. J. Pike, S. Froud, R. Wylde, B. Trociewitz, J. E. McKay, F. Mentink-Vigier, J. van Tol, S. Wi, W. W. Brey, J. R. Long, L. Frydman and S. Hill, A quasi-optical and corrugated waveguide microwave transmission system for simultaneous dynamic nuclear polarization NMR on two separate 14.1 T spectrometers, *J. Magn. Reson.*, 2018, **289**, 35–44.

14 Z. Gan, I. Hung, X. Wang, J. Paulino, G. Wu, I. M. Litvak, P. L. Gor'kov, W. W. Brey, P. Lendi, J. L. Schiano, *et al.*, NMR Spectroscopy up to 35.2 T Using a Series-Connected Hybrid Magnet, *J. Magn. Reson.*, 2017, **284**, 125–136.

15 C. Sauvée, M. Rosay, G. Casano, F. Aussenac, R. T. Weber, O. Ouari and P. Tordo, Highly Efficient, Water-Soluble Polarizing Agents for Dynamic Nuclear Polarization at High Frequency, *Angew. Chem., Int. Ed.*, 2013, **52**, 10858–10861.

16 G. Kresse and J. Hafner, Ab Initio Molecular Dynamics for Liquid Metals, *Phys. Rev. B: Condens. Matter Mater. Phys.*, 1993, **47**, 558–561.

17 P. Giannozzi, S. Baroni, N. Bonini, M. Calandra, R. Car, C. Cavazzoni, D. Ceresoli, G. L. Chiarotti, M. Cococcioni, I. Dabo, *et al.*, QUANTUM ESPRESSO: A Modular and Open-Source Software Project for Quantum Simulations of Materials, *J. Phys.: Condens. Matter*, 2009, **21**, 395502.

18 J. P. Perdew, K. Burke and M. Ernzerhof, Generalized Gradient Approximation Made Simple, *Phys. Rev. Lett.*, 1996, **77**, 3865–3868.

19 N. Troullier and J. L. Martins, Efficient Pseudopotentials for Plane-Wave Calculations, *Phys. Rev. B: Condens. Matter Mater. Phys.*, 1991, **43**, 1993–2006.

20 L. Kleinman and D. M. Bylander, Efficacious Form for Model Pseudopotentials, *Phys. Rev. Lett.*, 1982, **48**, 1425–1428.
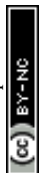
21 C. J. Pickard and F. Mauri, All-Electron Magnetic Response with Pseudopotentials: NMR Chemical Shifts, *Phys. Rev. B: Condens. Matter Mater. Phys.*, 2001, **63**, 245101.

22 P. Pyykkö, Year-2017 Nuclear Quadrupole Moments, *Mol. Phys.*, 2018, **116**, 1328–1338.

23 L. Mayen, N. D. Jensen, M. Desbord, D. Laurencin, C. Gervais, C. Bonhomme, M. E. Smith, F. Porcher, E. Elkaim, C. Charvillat, P. Gras, C. Rey, J. Soulié and C. Combes, Advances in the synthesis and structure of α-canaphite: a multitool and multiscale study, *CrystEngComm*, 2020, **22**, 3130–3143.

24 (*a*) E. Davies, M. J. Duer, S. E. Ashbrook and J. M. Griffin, Applications of NMR Crystallography to Problems in Biomineralization: Refinement of the Crystal Structure and ^{31}P Solid-State NMR Spectral Assignment of Octacalcium Phosphate, *J. Am. Chem. Soc.*, 2012, **134**, 12508–12515; (*b*) D. Laurencin, Y. Li, M. Duer, D. Iuga, C. Gervais and C. Bonhomme, A [43]Ca NMR perspective on octacalcium phosphate and its hybrid derivatives, *Magn. Reson. Chem.*, 2021, **59**, 1048–1061.

25 Z. Zou, W. J. E. M. Habraken, G. Matveeva, A. C. S. Jensen, L. Bertinetti, M. A. Hood, C.-Y. Sun, P. U. P. A. Gilbert, I. Polishchuk, B. Pokroy, J. Mahamid, Y. Politi, S. Weiner, P. Werner, S. Bette, R. Dinnebier, U. Kolb, E. Zolotoyabko and P. Fratzl, A hydrated crystalline calcium carbonate phase: Calcium carbonate hemihydrate, *Science*, 2019, **363**, 396–400.